

Geometry and torsional energies of a C–C-protonated *n*-alkane

Qingbin Li, Ken C. Hunter, Christa Seitz, and Allan L. L. East

Department of Chemistry and Biochemistry, University of Regina, Regina, Saskatchewan, Canada S4S 0A2

(Received 9 June 2003; accepted 18 July 2003)

The geometry and relative energies of torsional conformers of centrally protonated $C_4H_{11}^+$ were studied with *ab initio* methods, to (a) obtain the most accurate geometry of the three-center–two-electron CHC bond to date, (b) evaluate the performance of lower levels of approximation upon this challenging structure, and (c) gain an understanding of the torsional dynamics of $C_4H_{11}^+$. Twenty-nine combined levels of theory were used to optimize the geometry of the C_2 -symmetry minimum for *trans*- $C_4H_{11}^+$, and the most accurate one [CCSD(T)/cc-pVTZ] gave the following CHC bond geometry: $\theta_{CHC} = 122.4^\circ$, $R_{CC} = 2.177 \text{ \AA}$, $R_{CH} = 1.2424 \text{ \AA}$. Molecular-orbital-based methods generally perform better than density functional methods for describing the three-center–two-electron bond. A smaller subset of levels of theory was used to optimize other torsional conformers of centrally protonated $C_4H_{11}^+$, varying the CCCC dihedral (*trans*, *gauche*, *cis*) and the dihedral for the bridging proton (various eclipsed and staggered positions). The results show that all conformers lie within a 4 kJ mol^{-1} range, with the lowest-energy conformer being either *trans* or *gauche* with a staggered dihedral for the bridging proton. The effect of core-valence correlation was also investigated. Finally, the potential energy surface as a function of the CCCC and bridging-proton dihedral angles was qualitatively estimated and drawn, based on our computed data, to aid in understanding the fluxional character of $C_4H_{11}^+$. © 2003 American Institute of Physics. [DOI: 10.1063/1.1607959]

I. INTRODUCTION

Protonated alkanes (alkanium or carbonium ions, acyclic $C_xH_{2x+3}^+$) are gas-phase ions of very short lifetimes, originally detected and studied via mass spectrometry experiments.^{1–16} Only two gas-phase infrared spectra have been reported to date.^{17,18} They have never been directly detected in solution, although the idea has been greatly popularized by Olah, following his initial reactions of alkanes with superacids,^{19–22} and by Haag and Dessau, who incorporated them into catalytic cracking mechanisms.^{23,24}

There are now several published computational chemistry studies of geometric parameters of protonated alkanes, and none from experiment. The minimum-energy structures in the gas phase contain a three-center–two-electron (3c2e) bond, either CHC or CHH. For $C_2H_7^+$, the lowest-energy structure features a triangular CHC 3c2e bond; calculations at moderate levels of theory (MP2, BLYP, B3LYP) produce values for the 3c2e CHC angle of 106° – 114° .^{25–28} For larger protonated alkanes, the lowest-energy forms feature the extra H atom bridging two carbons of the highest substitution (quaternary, tertiary, etc.), and these forms are, paradoxically, the least stable ones, leading to dissociation quite readily. The literature reports of geometrical parameters for these larger systems will be summarized here.

In 1996 Collins and O'Malley reported a comparison of semiempirical and *ab initio* methods for selected conformers of dissociated-complex and C–C-protonated forms of $C_3H_9^+$, $C_4H_{11}^+$, and neo- $C_5H_{13}^+$,²⁶ which included their initial data on $C_3H_9^+$ from 1994.²⁷ Although not stressed, the reported geometric parameters for the 3c2e bond of C–C-protonated forms demonstrate greater disagreement among

ab initio methods than was seen for $C_2H_7^+$, with MP2 angles below 130° , B3LYP ones near 136° , and BLYP ones above 150° . They also reported results from semiempirical methods, and while their AM1 angles were 141° – 154° , their PM3 angles were 174° – 180° , notably inferior in quality and similar to older MINDO/3 results.^{29,30} In 1997, single isomers of larger systems were featured in two papers concerned with hydride transfer from alkanes to carbenium ions: Frash, Solkan, and Kazansky published MP2 geometries of centrally protonated butane, 2,3-dimethylbutane and 2,2,3,3-tetramethylbutane,³¹ and Boronat, Viruela, and Corma optimized centrally protonated di-, tri-, and tetramethylbutane with B3LYP, B3PW91, and MP2.³² Their structures indicate that the 3c2e CHC angle is greatly increased with increasing methyl substitution, regardless of level of theory employed. Also that year, Mota and co-workers reported several MP2 and B3LYP structures of conformers of protonated isobutane,³³ and later published results from MP2 structures of $C_3H_9^+$,³⁴ *n*- $C_4H_{11}^+$,³⁵ and protonated adamantane ($C_{10}H_{17}^+$).³⁶ Our group has reported some 3c2e-bond geometry parameters from MP2 and B3LYP optimizations of protonated all-*trans* *n*-alkanes up to $C_{14}H_{31}^+$,³⁷ and from 39 MP2-optimized isomers of $C_8H_{19}^+$.³⁸

While all of these authors, and others, have gone on to simulate these ions as possible intermediates in reactions of alkanes with acidic catalyst models, there are two holes in the basic understanding of protonated alkanes that we would like to fill in this report. First, despite a demonstrated disagreement between moderate levels of theory on the exact 3c2e-bond geometries,^{26,32,37} there is to date no published structure for a C–C-protonated alkane using the coupled-cluster approximation [CCSD(T)] or any other high-accuracy

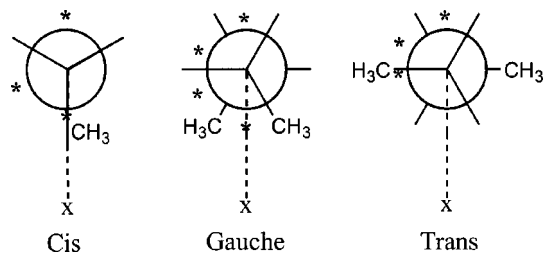


FIG. 1. Newman projections of *cis*, *gauche*, and *trans* butane, with asterisks to denote the dihedral positions chosen for the extra proton in $C_4H_{11}^+$ geometry optimizations.

method. Second, although several papers have presented a great number of optimized structures for these ions, implying a great deal of fluxionality, a good qualitative discussion of the fluxionality of the 3c2e bond is lacking. Knowing an accurate geometrical structure for a protonated *n*-alkane will be of use for spectroscopists and for computational modelers who wish to test less-extensive approximations for use on modeling larger systems.

This study addresses these two points for the case of a protonated C–C bond between two secondary-substituted carbon atoms. We previously computed a CCSD(T) optimization of a $C_4H_{11}^+$ conformation, and noticed that the C–H–C angle at the 3c2e bond is very sensitive to different levels of theory, but did not go into great detail.³⁸ Therefore, the centrally protonated *trans*- $C_4H_{11}^+$ ion is chosen here as the object molecule whose geometry is studied in depth. For the fluxionality study, we have computed the structure and energy of other conformers that arise from variations in two particular dihedral angles: one for the carbon skeleton (Φ_{CCCC}) and one for the revolution of the bridging proton around its C–C skeleton (Φ_{HCCX}). Included in the fluxionality study is an investigation of the effect of core-valence correlation upon geometries and energies.

II. THEORETICAL METHODS

All calculations were performed using the software suite GAUSSIAN 98,³⁹ with the exception of the coupled-cluster calculations for which we used the MOLPRO 2002 package.⁴⁰ Molecular electronic energies, optimized geometries, and vibrational frequencies for several $C_4H_{11}^+$ conformers were calculated, and point-group symmetry was used where applicable. The optimized geometries were characterized as

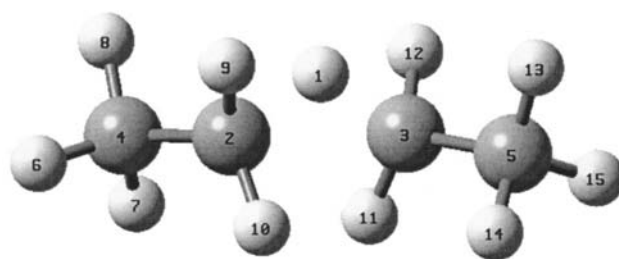


FIG. 2. Atom numbering for the *trans*- $\mu 23(180^\circ)$ configuration of $C_4H_{11}^+$.

minima or transition states on the potential energy surface by the absence of imaginary vibrational frequencies or the presence of a single one, respectively. Relative conformer energies are not corrected for zero-point effects.

Ten levels of electronic structure theory were employed. Two density functional theory (DFT) methods were tried: the semiempirical B3LYP (Becke-3 exchange⁴¹ and Lee–Yang–Parr correlation⁴² functionals) and the *ab initio* PW91 (both functionals from Perdew and Wang⁴³). Hartree–Fock-based methods include Hartree–Fock (HF), Møller–Plesset perturbation theory to second and third order (MP2 and MP3),⁴⁴ configuration interaction (CISD),^{45,46} and coupled-cluster methods [CCSD, CCSD(T)].^{47–50} Effects of the DFT numerical integration grid were tested with B3LYP, and effects of the frozen-core approximation were tested with MP2.

Eleven basis sets were tested: the seven Pople basis sets were STO-3G, 6-31G, 6-31G(*d*), 6-31G(*d,p*), 6-311G(*d*), 6-311+G(2*df,p*), and 6-311+G(3*df,2p*),^{39,51} and the four Dunning basis sets were cc-pVDZ, cc-pVTZ, cc-pVQZ, and cc-pCVTZ.^{52,53}

A naming system is used to keep track of the various conformers of centrally protonated *n*-butane. The $\mu 23$ designation indicates that the extra proton bridges the central C₂–C₃ bond of *n*-butane. Its conformers arise from variations in two particular dihedral angles: one for the carbon skeleton (Φ_{CCCC}) and one for the revolution of the bridging proton around its C–C skeleton (Φ_{HCCX}). Figure 1 demonstrates how Φ_{HCCX} is measured; we take X to be the position that bisects the CCCC dihedral angle in the Newman projection (straight down in the figure), and the proton dihedral angle is measured relative to it. This definition maximizes the use of symmetry, as will be seen in the surface plots of

TABLE I. Shorthand notation for basis sets and methods used.

Shorthand	Basis set	Basis set size ^a	Shorthand	Method
B1	STO-3G	93/31	M1	HF
B2	6-31G	132/56	M2	B3LYP, fine grid
B3	6-31G(<i>d</i>)	156/82	M3	B3LYP, ultrafine grid
B4	6-311G(<i>d</i>)	183/105	M4	PW91, fine grid
B5	cc-pVDZ	209/111	M5	MP2
B6	6-31G(<i>d,p</i>)	189/115	M6	MP2(full)
B7	6-311+G(2 <i>df,p</i>)	296/202	M7	MP3
B8	6-311+G(3 <i>df,2p</i>)	353/255	M8	CISD
B9	cc-pVTZ	399/274	M9	CCSD
B10	cc-pVQZ	775/550	M10	CCSD(T)

^aNumber of primitive Gaussians/number of contracted Gaussians.

TABLE II. Optimized geometries of the *trans*- μ 23(180°) isomer of $C_4H_{11}^+$, from the four highest-accuracy levels of theory used in this work.^a

Parameter	cc-pVTZ MP2	cc-pVQZ MP2	6-31G(<i>d,p</i>) CCSD(T)	cc-pVTZ CCSD(T)
$R(C_2H_1)$	1.2340	1.2329	1.2393	1.2424
$R(C_2C_3)$	2.113	2.096	2.268	2.177
$R(C_4C_2)$	1.4964	1.4944	1.5024	1.5015
$R(H_6C_4)$	1.0916	1.0903	1.0949	1.0948
$R(H_7C_4)$	1.0860	1.0850	1.0891	1.0892
$R(H_8C_4)$	1.0861	1.0851	1.0884	1.0890
$R(H_9C_2)$	1.0932	1.0924	1.0920	1.0941
$R(H_{10}C_2)$	1.0821	1.0810	1.0855	1.0847
$\theta(C_3H_1C_2)$	117.7	116.4	132.4	122.4
$\theta(C_4C_2C_3)$	108.9	108.9	108.6	108.6
$\theta(H_6C_4C_2)$	106.3	106.4	105.9	106.2
$\theta(H_7C_4C_2)$	112.3	112.3	112.2	112.2
$\theta(H_8C_4C_2)$	112.2	112.2	112.1	112.1
$\theta(H_9C_2C_3)$	113.6	113.9	111.1	113.1
$\theta(H_{10}C_2C_3)$	86.3	86.4	86.7	86.0
$\Phi(C_4C_2C_3H_1)$	94.2	94.6	91.8	93.5
$\Phi(H_6C_4C_2C_3)$	164.6	164.9	164.2	164.4
$\Phi(H_7C_4C_2C_3)$	46.9	47.1	46.8	46.8
$\Phi(H_8C_4C_2C_3)$	-77.8	-77.5	-78.2	-78.0
$\Phi(H_9C_2C_3C_5)$	57.0	57.8	53.5	56.1
$\Phi(H_{10}C_2C_3C_5)$	-54.0	-53.1	-58.9	-55.5

^aBond lengths R in Å, angles θ and dihedral angles Φ in degrees.

the potential energy surface (PES). The asterisks indicate the various initial positions chosen for the bridging proton; not all of these corresponded to stationary points on the PES. To designate particular conformers, the Φ_{CCCC} positions 0°, 60°, and 180° are designated with the familiar terms *cis*, *gauche*, and *trans*, while the Φ_{HCCX} position is indicated with the approximate angle in brackets. For instance, *gauche*- μ 23(60°) refers to an asymmetric structure in which $\Phi_{CCCC} = 60^\circ$ and $\Phi_{HCCX} = 60^\circ$. Exact values of these angles are not used in the nomenclature since they are dependent upon the level of theory employed in the geometry optimization.

III. RESULTS AND DISCUSSION

A. Effects of various levels of theory upon the geometry

This first study investigated the effects of basis set and method upon the optimized geometrical structure of one particular C–C-protonated *n*-alkane conformer: namely, the

C_2 -symmetry *trans*- μ 23(180°) conformer of $C_4H_{11}^+$. Table I lists the ten basis sets tested with the B3LYP and MP2 methods (M2 and M5, respectively) and the ten methods tested with the 6-31G(*d,p*) basis set (B6). In addition to these 28 runs, we performed a long one with M10/B9 [CCSD(T)/cc-pVTZ], requiring 31 days on our fastest computer with MOLPRO, to provide the most accurate geometry to date as a benchmark. All optimizations were performed with C_2 symmetry, but the optimizations with B2 (6-31G) and one with B3 [B3LYP/6-31G(*d*)] had to be finished in C_{2h} due to the lack of a C_2 structure, and the optimizations with B1 (STO-3G) were discarded because they resulted in a *gauche* structure. Figure 2 shows the atom numbering we used for labeling the internal coordinates.

Table II displays the resulting geometries from our four highest-accuracy calculations (M5/B9, M5/B10, M10/B6, and M10/B9). The best level of theory, CCSD(T)/cc-pVTZ, produced a $\theta(C_3H_1C_2)$ angle of 122.4°, an $R(C_2C_3)$ of 2.177 Å, and an $R(C_2H_1)$ of 1.2424 Å, which now serves as the best prediction of the 3c2e bond geometry for protonated secondary–secondary carbon bonds. This geometry is not reproduced well by the other three levels of theory shown in this table.

Table III compares the effect of basis set upon a subset of internal coordinate values, from MP2 optimizations. Basis set convergence does not begin to appear until the triple-zeta basis sets with full polarization (B7–B9). Compared to the ideal B10 (cc-pVQZ) result, the 6-31G basis set (B2) gives generally poor results, especially for the $\theta(C_3H_1C_2)$ bridging angle which shows a basis set error of over 60°. Dihedral angles using B7–B10 seem improved by 2°–3° over those from smaller basis sets. The coordinates most sensitive to basis set, however, are $R(C_2C_3)$ and $\theta(C_3H_1C_2)$, which are involved in the 3c2e bond. Larger bases sets favor smaller values for both of these coordinates. Figure 3 plots the $\theta(C_3H_1C_2)$ data for a clearer sense of scale and includes the results from B3LYP optimizations. Note that, while B3LYP and MP2 results clearly disagree with each other, the trend in basis set error with either method is generally the same, once polarization functions on hydrogen are in place (from cc-pVDZ on). Also note that the generally reliable double-zeta basis sets with polarization functions (B3, B5, B6) are not

TABLE III. Selected parameters from the optimized geometries of the *trans*- μ 23(180°) isomer of $C_4H_{11}^+$, using the MP2 method and various basis sets.^a

Parameter	B2	B3	B4	B5	B6	B7	B8	B9	B10
$R(C_2H_1)$	1.2510	1.2386	1.2357	1.2450	1.2317	1.2363	1.2337	1.2340	1.2329
$R(C_2C_3)$	2.502	2.250	2.158	2.186	2.204	2.129	2.113	2.113	2.096
$R(C_4C_2)$	1.5105	1.4978	1.5004	1.5036	1.4975	1.4950	1.4966	1.4964	1.4944
$\theta(C_3H_1C_2)$	180.0	130.5	121.7	122.8	127.0	118.9	117.8	117.7	116.4
$\theta(C_4C_2C_3)$	108.0	109.0	109.3	109.1	109.0	109.0	108.8	108.9	108.9
$\theta(H_9C_2C_3)$	98.9	111.7	113.3	112.4	111.9	113.5	113.7	113.6	113.9
$\theta(H_{10}C_2C_3)$	98.9	86.5	86.1	86.1	86.5	86.3	86.4	86.3	86.4
$\Phi(C_4C_2C_3H_1)$	b	92.1	93.2	92.9	92.4	93.9	94.3	94.2	94.6
$\Phi(H_9C_2C_3C_5)$	57.7	53.6	54.9	54.9	54.0	56.4	57.4	57.0	57.8
$\Phi(H_{10}C_2C_3C_5)$	-57.7	-58.3	-56.1	-56.5	-57.8	-54.6	-53.7	-54.0	-53.1

^aBond lengths R in Å, angles θ and dihedral angles Φ in degrees.

^bThis coordinate is not defined for this C_{2h} -symmetry structure.

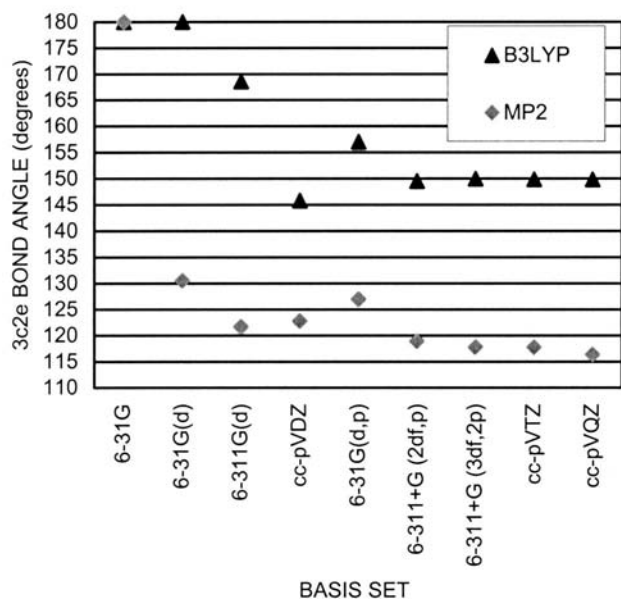


FIG. 3. Effect of basis set upon optimized $\theta(\text{C}_3\text{H}_1\text{C}_2)$ for the *trans*- $\mu_{23}(180^\circ)$ configuration.

sufficient for basis set convergence of this 3c2e bond parameter.

Table IV compares the effect of method upon a subset of several internal coordinate values, using the 6-31G(*d,p*) basis set. Compared to the ideal CCSD(T) (M10) result, the Hartree–Fock method (M1) gives surprisingly good results. The density functional methods employed here (M2–M4) give results that are qualitative, but not quantitative, and not just for the coordinates of the 3c2e bond. For instance, the DFT methods give $\Phi(\text{C}_4\text{C}_2\text{C}_3\text{H}_1)$ dihedral angles of less than 90° , which puckers the carbon skeleton up towards the bridging proton rather than away, in disagreement with the higher-level methods. Variances between these DFT methods and other methods for other coordinates such as $\theta(\text{H}_{10}\text{C}_2\text{C}_3)$ and $\Phi(\text{C}_4\text{C}_2\text{C}_3\text{H}_1)$ are related to this puckering. Use of a finer integration grid (M3 versus M2) produced very little improvement, as expected. Variances among all methods can be seen in the sensitive 3c2e coordinates, with the DFT methods producing the worst description of the 3c2e bond. Figure 4 plots the $\theta(\text{C}_3\text{H}_1\text{C}_2)$ data for a clearer sense of

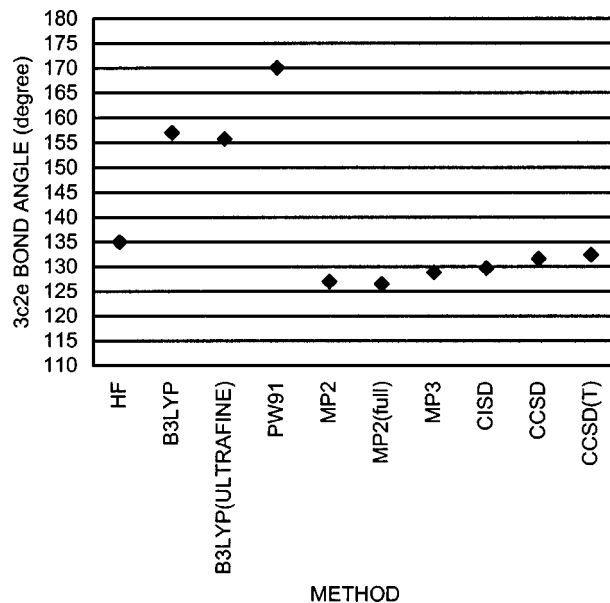


FIG. 4. Effect of the electron correlation method upon optimized $\theta(\text{C}_3\text{H}_1\text{C}_2)$ for the *trans*- $\mu_{23}(180^\circ)$ configuration.

scale; note that the DFT methods produced angles over 20° greater than CCSD(T), and improvements to the level of sophistication among HF-based methods increased this angle from 127° (MP2) to 132° (CCSD(T)).

When comparing the geometries in Tables II and III to the most accurate one, CCSD(T)/cc-pVTZ of Table I, we find that lower levels of theory can be used with excellent results, because of a cancellation of basis set and method errors for the 3c2e bond. In particular, combining the MP2 method with either the 6-311G(*d*) or cc-pVDZ basis sets (the B4 and B5 columns in Table I) can provide good accuracy in geometrical structure and hence be used for the modeling of larger systems.

B. Effects of various levels of theory upon torsional energies

Several combined levels of theory [including CCSD(T)/6-31G(*d,p*) and MP2/6-31G(*d*)] were selected and used to optimize other torsional structures of $\mu_{23}\text{-C}_4\text{H}_{11}^+$, varying the Φ_{CCCC} dihedral (*trans*, *gauche*,

TABLE IV. Selected parameters from the optimized geometries of the *trans*- $\mu_{23}(180^\circ)$ isomer of $\text{C}_4\text{H}_{11}^+$, using the 6-31G(*d,p*) basis set and various electronic structure methods.^a

Parameter	M1	M2	M3	M4	M5	M6	M7	M8	M9	M10
$R(\text{C}_2\text{H}_1)$	1.2512	1.2630	1.2629	1.2685	1.2317	1.2299	1.2330	1.2320	1.2362	1.2393
$R(\text{C}_2\text{C}_3)$	2.312	2.475	2.469	2.528	2.204	2.196	2.224	2.231	2.255	2.268
$R(\text{C}_4\text{C}_2)$	1.5026	1.4903	1.4905	1.4846	1.4975	1.4960	1.5012	1.4980	1.5016	1.5024
$\theta(\text{C}_3\text{H}_1\text{C}_2)$	135.0	157.0	155.8	170.1	127.0	126.5	128.8	129.7	131.6	132.4
$\theta(\text{C}_4\text{C}_2\text{C}_3)$	108.7	109.3	109.2	109.0	109.0	109.1	108.7	108.8	108.7	108.6
$\theta(\text{H}_9\text{C}_2\text{C}_3)$	111.1	103.9	104.3	100.2	111.9	112.1	112.1	112.0	111.4	111.1
$\theta(\text{H}_{10}\text{C}_2\text{C}_3)$	86.9	91.4	91.1	94.8	86.5	86.5	86.5	86.6	86.7	86.7
$\Phi(\text{C}_4\text{C}_2\text{C}_3\text{H}_1)$	89.8	85.1	86.4	87.0	92.4	92.4	92.5	91.7	91.8	91.8
$\Phi(\text{H}_9\text{C}_2\text{C}_3\text{C}_5)$	50.0	44.1	46.5	50.1	54.0	54.1	54.4	52.9	53.4	53.5
$\Phi(\text{H}_{10}\text{C}_2\text{C}_3\text{C}_5)$	-62.9	-70.0	-67.6	-64.6	-57.8	-57.6	-57.7	-59.3	-58.9	-58.9

^aBond lengths R in Å, angles θ and dihedral angles Φ in degrees.

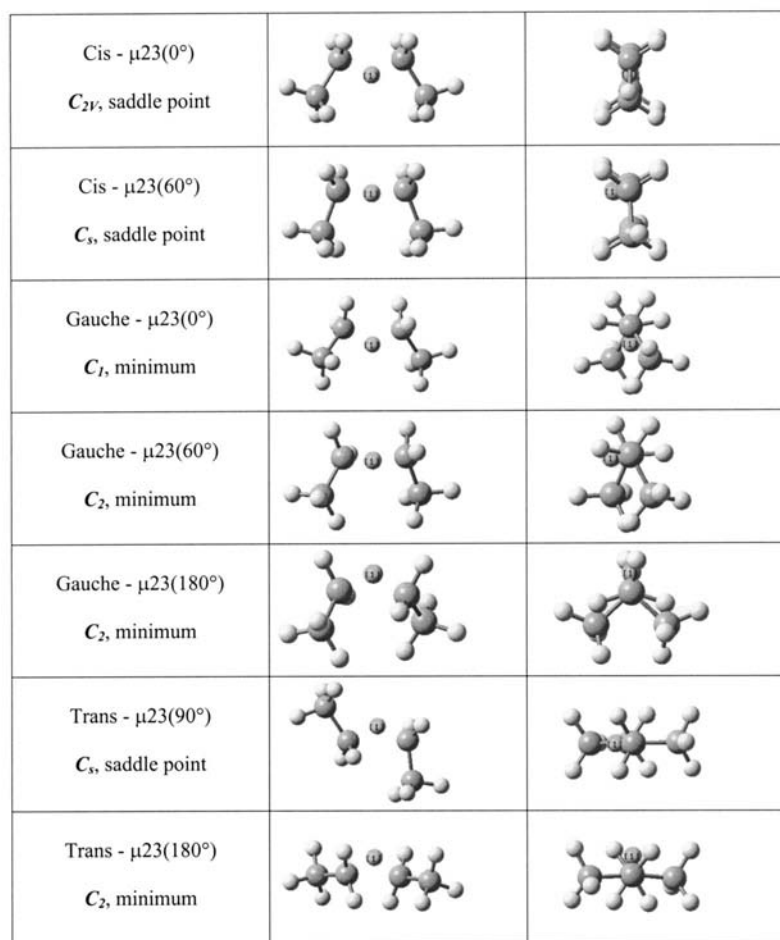


FIG. 5. MP2/cc-pVTZ optimized conformers of centrally protonated butonium ion, viewed from two directions.

cis) and the Φ_{HCCX} dihedral for the bridging proton (various eclipsed and staggered positions) as described in the Methods section. Of interest here are the relative energies, rather than the optimized geometrical structures. Between four and seven of the ten tested conformers resulted in stationary points, depending on the level of theory employed, and several correspond to torsional transition states.

Figure 5 shows the images of the seven optimized geometries obtained from MP2/cc-pVTZ, including point-group symmetry and the nature of the structure (minimum or

saddle point on the PES). The two *cis* structures are transition states for interconversion between two *gauche* structures. The *trans-μ23(90°)* structure is a transition state for revolution of the bridging H atom about the central C–C bond. Table V displays the optimized values for the torsional angles obtained with two different levels of theory, to demonstrate (i) that the actual angles vary from the idealized descriptions (0° , 60° , 90° , etc.) and (ii) that different levels of theory will greatly disagree with each other on actual torsional angles for protonated alkanes.

TABLE V. Geometrical parameters of various $\text{C}_4\text{H}_{11}^+$ conformers.^a

Conformer	Point group	Imaginary frequencies	MP2 cc-pVTZ		CCSD(T) 6-31G(<i>d,p</i>)	
			Φ_{CCCC}	Φ_{HCCX}	Φ_{CCCC}	Φ_{HCCX}
<i>cis-μ23(0°)</i> ^b	C_{2v}	1 (in Φ_{CCCC})	0°	0°	0°	0°
<i>cis-μ23(60°)</i> ^b	C_s	1 (in Φ_{CCCC})	0°	82°	0°	51°
<i>gauche-μ23(0°)</i>	C_2	0	59°	0°	58°	0°
<i>gauche-μ23(60°)</i>	C_1	0	50°	84°	51°	74°
<i>gauche-μ23(180°)</i>	C_2	0	94°	180°	91°	180°
<i>trans-μ23(90°)</i> ^b	C_s	1 (in Φ_{HCCX})	180°	90°	180°	90°
<i>trans-μ23(180°)</i>	C_2	0	172°	180°	176°	180°

^aThe reported angles are dihedrals about the $\text{C}_2\text{--C}_3$ bond. Φ_{HCCX} measures the dihedral angle of the bridging hydrogen atom measured from a point X which bisects the Φ_{CCCC} dihedral; therefore, $\Phi_{\text{HCCX}}=0^\circ$ or 180° results in the molecule maintaining a C_2 rotation axis.

^bSaddle point (not a minimum) on the potential energy surface.

TABLE VI. Relative energies (kJ mol⁻¹) of various of C₄H₁₁⁺ conformers.^a

Conformer	B3LYP 6-31G(<i>d</i>)	MP2 6-31G(<i>d</i>)	MP2(full) 6-31G(<i>d,p</i>)	MP2 cc-pVTZ	CCSD(T) 6-31G(<i>d,p</i>)
<i>cis</i> -μ23(0°) ^b	-0.02	2.05	3.04	4.91	2.19
<i>cis</i> -μ23(60°) ^b	Does not exist	Does not exist	Does not exist	5.35	2.45
<i>gauche</i> -μ23(0°)	-0.69	-0.66	-0.01	1.80	-0.22
<i>gauche</i> -μ23(60°)	Does not exist	-0.56	-0.13	0.36	-0.29
<i>gauche</i> -μ23(180°)	Does not exist	3.70	4.32	4.30	3.21
<i>trans</i> -μ23(90°) ^b	0.03	2.41	3.47	5.14	2.34
<i>trans</i> -μ23(180°)	0.00	0.00	0.00	0.00	0.00

^aThe absolute energies in atomic units for the *trans*-μ23(180°) conformer are -158.72312 [B3LYP/6-31G(*d*)], -158.07236 [MP2/6-31G(*d*)], -158.18186 [MP2(full)/6-31G(*d,p*)], -158.32545 (MP2/cc-pVTZ), and -158.24172 [CCSD(T)/6-31G(*d,p*)].

^bSaddle point (not a minimum) on the potential energy surface.

Table VI shows the relative energies of these torsional structures, from our five different levels of theory tested. Note the disagreement as to which conformer is the lowest-energy one: with CCSD(T)/6-31G(*d,p*) it is *gauche*-μ23(60°), but with MP2/cc-pVTZ it is *trans*-μ23(180°), and with MP2/6-31G(*d*) it is *gauche*-μ23(0°). These three minima do appear to be generally lower in energy than the other four structures, although B3LYP/6-31G(*d*) appears to have qualitative difficulties in this regard. The data suggest that the bridging H atom prefers staggered positions, but the question of *which* staggered positions it prefers is a question without a simple answer.

Table VII presents a study of core-valence correlation effects, showing the relative energies of these seven structures reoptimized with three other relevant levels of theory. The differences in geometry were quite insignificant. The cc-pCVTZ basis set provides extra functions for core electron regions to improve the reliability of correlation methods which include core-valence correlation, such as MP2(full). Comparison of the first two columns of the table shows the negligible effect of adding core functions to a procedure that does not include core-valence correlation. These columns also agree very well (within 0.3 kJ mol⁻¹) with the fourth column, which features core-valence correlation with the appropriate basis set; this indicates that the incorporation of core-valence correlation has virtually no effect on these relative torsional energies. The third column demonstrates the

TABLE VII. Relative energies (kJ mol⁻¹) of various C₄H₁₁⁺ conformers, testing core-valence correlation.^a

Conformer	MP2 cc-pVTZ	MP2 cc-pCVTZ	MP2(full) cc-pVTZ	MP2(full) cc-pCVTZ
<i>cis</i> -μ23(0°) ^b	4.91	4.97	4.43	5.22
<i>cis</i> -μ23(60°) ^b	5.35	5.39	5.39	5.52
<i>gauche</i> -μ23(0°)	1.80	1.86	1.15	2.07
<i>gauche</i> -μ23(60°)	0.36	0.38	0.16	0.44
<i>gauche</i> -μ23(180°)	4.30	4.29	4.24	4.33
<i>trans</i> -μ23(90°) ^b	5.14	5.21	4.87	5.38
<i>trans</i> -μ23(180°)	0.00	0.00	0.00	0.00

^aThe absolute energies in atomic units for the *trans*-μ23(180°) conformer are -158.32545 (MP2/cc-pVTZ), -158.33001 (MP2/cc-pCVTZ), -158.38996 [MP2(full)/cc-pVTZ], and -158.52009 [MP2(full)/cc-pCVTZ].

^bSaddle point (not a minimum) on the potential energy surface.

effect of invoking core-valence correlation without supplementing a basis set appropriately, and the effects are more noticeable, but the deviations are less than 1 kJ mol⁻¹ and the energy ordering does not change.

C. Plots of the torsional PES

The data of Table VI indicate that the torsional PES is more complicated than anticipated. We strove to further our understanding of the fluxionality of μ23-C₄H₁₁⁺ by plotting plausible two-dimensional (2D) PES functions $E(\Phi_{\text{CCCC}}, \Phi_{\text{HCCX}})$ that fit the data. We began with the general Fourier series expansion

$$\begin{aligned}
 E(\Phi_C, \Phi_H) = & \sum_{m=0}^{\infty} \sum_{n=0}^{\infty} A_{mn} \cos\left(\frac{m}{2}\Phi_C\right) \cos(n\Phi_H) \\
 & + B_{mn} \sin\left(\frac{m}{2}\Phi_C\right) \sin(n\Phi_H) \\
 & + C_{mn} \cos\left(\frac{m}{2}\Phi_C\right) \sin(n\Phi_H) \\
 & + D_{mn} \sin\left(\frac{m}{2}\Phi_C\right) \cos(n\Phi_H),
 \end{aligned}$$

where Φ_C and Φ_H are shorthand for Φ_{CCCC} and Φ_{HCCX} , respectively. The factor of 1/2 in the $m\Phi_C$ terms is due to the fact that $E(\Phi_C, \Phi_H) = E(\Phi_C + 4\pi, \Phi_H)$, but not $E(\Phi_C + 2\pi, \Phi_H)$ in general, with our coordinate definitions. We forced this function to obey the symmetry of the problem by applying three symmetry rules, listed in Table VIII; these reduce the expression to

TABLE VIII. Symmetry effects on the PES function $E(\Phi_{\text{CCCC}}, \Phi_{\text{HCCX}})$.

Symmetry rule	Consequence
$E(-\Phi_C, \Phi_H) = E(\Phi_C, \Phi_H)$	No $\sin\left(\frac{m}{2}\Phi_C\right)$ terms
$E(\Phi_C, -\Phi_H) = E(\Phi_C, \Phi_H)$	No $\sin(n\Phi_H)$ terms
$E\left(\pi - \Phi_C, \frac{\pi}{2} - \Phi_H\right) = E\left(\pi + \Phi_C, \frac{\pi}{2} + \Phi_H\right)$	$(m+n)$ must be even

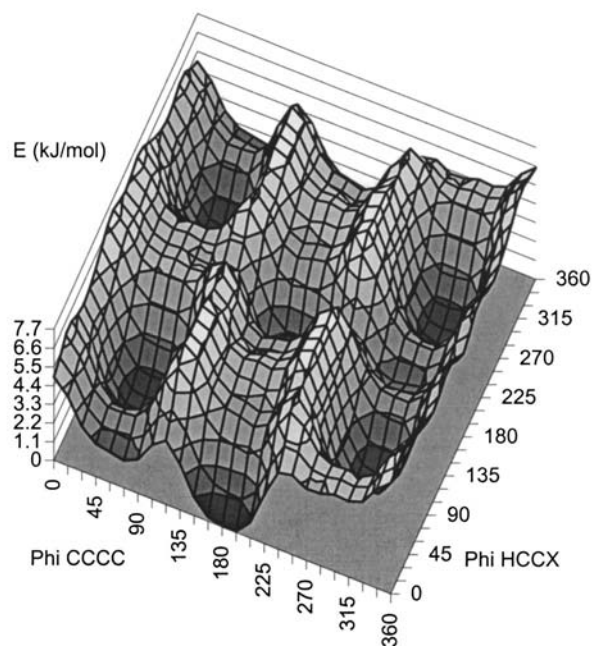
TABLE IX. Coefficients (kJ mol^{-1}) from least-squares fitting for $E(\Phi_C, \Phi_H)$.

Coefficient	MP2	CCSD(T)
	cc-pVTZ	6-31G(<i>d,p</i>)
$A_{0,0}$	3.899 57	2.490 01
$A_{2,0}$	-0.488 38	-0.449 30
$A_{1,1}$	-0.916 01	-1.666 06
$A_{0,2}$	-0.007 03	-0.239 37
$A_{4,0}$	0.268 13	-0.117 46
$A_{3,1}$	-0.216 30	-0.472 08
$A_{2,2}$	1.649 47	1.231 26
$A_{1,3}$	-0.184 68	-0.299 30
$A_{0,4}$	-0.580 30	-0.296 87
$A_{6,0}$	1.778 09	1.538 72
$A_{4,2}$	-0.778 49	-0.148 76
$A_{2,4}$	0.210 22	0.083 53
$A_{0,6}$	-0.320 70	-0.172 46
$A_{5,1}$	0.399 22	0.338 19
$A_{3,3}$	0.190 85	0.422 04
$A_{1,5}$	-0.072 17	0.117 00
$A_{6,2}$	-0.506 00	-0.509 85
$A_{2,6}$	0.186 50	-0.023 70
$A_{12,0}$	0.507 76	0.271 41
$A_{12,2}$	-0.110 18	0.092 74

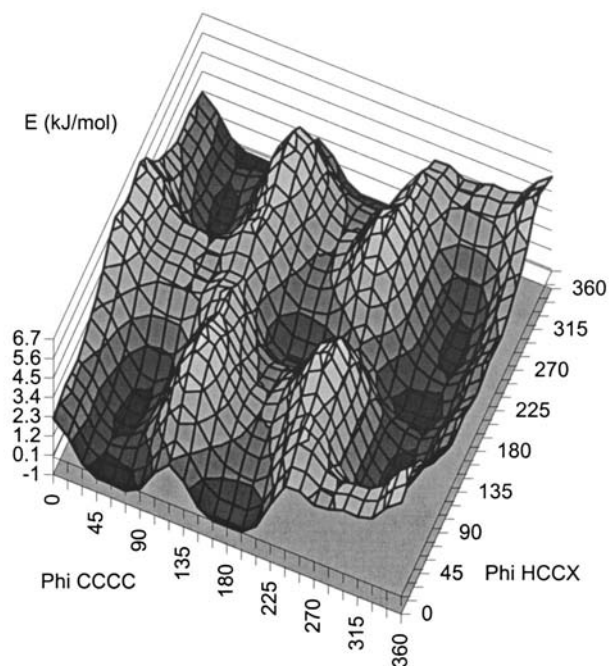
$$E(\Phi_C, \Phi_H) = \sum_{m=0}^{\infty} \sum_{n=0}^{\infty} A_{mn} \cos\left(\frac{m}{2}\Phi_C\right) \cos(n\Phi_H),$$

where $m+n$ must be even. Truncated versions of this function were subject to least-squares fitting to the MP2/cc-pVTZ seven-point dataset (energies in Table VI, coordinate values in Table V), to find optimized values for the A_{mn} coefficients. We found that we needed far more than seven terms in the double sum to produce an appropriate looking function. We eventually settled on a function of 20 terms. Of course, we found many successful fits to the limited dataset. One could try to compute more points on the PES to obtain a better-defined fit, but these would be nonstationary points requiring restricted optimizations, and due to the approximate nature of the data, we considered this extra work to be of very little benefit. Instead, a handful of the successful but underdetermined fitted functions were plotted graphically, and one physically reasonable function was chosen for presentation. This provides a reasonable approximation to the shape of this coupled PES, for the purposes of discussing fluxional dynamics of a protonated n -alkane.

Two such PES functions were generated, which represent MP2/cc-pVTZ and CCSD(T)/6-31G(*d,p*) data, respectively. These functions appear in Table IX, and surface plots of these functions appear in Figs. 6 and 7. One can see long valleys for *gauche* and *trans* structures ($\Phi_{\text{CCCC}} = 60^\circ, 180^\circ, 300^\circ$), which indicates that revolution of the H atom around the C–C bond is extremely facile. Interconversion between *trans* and *gauche* conformers can occur most easily between *trans*- $\mu 23(180^\circ)$ and *gauche*- $\mu 23(0^\circ)$, which can be visually seen in the plots as either $(180^\circ, 180^\circ) \rightarrow (300^\circ, 180^\circ)$, $(180^\circ, 0^\circ) \rightarrow (60^\circ, 0^\circ)$, or $(180^\circ, 360^\circ) \rightarrow (60^\circ, 360^\circ)$, all identical by symmetry. This particular interconversion channel is a visual indication that the two torsional motions are significantly coupled. In fact, in some

FIG. 6. 3D surface plot of the 2D torsional potential energy surface $E(\Phi_{\text{CCCC}}, \Phi_{\text{HCCX}})$, using MP2/cc-pVTZ data.

geometry optimizations we observed coupling of a third coordinate, the distance of the bridging H from the center of the C–C bond, because in some optimizations the proton moved into the C–C bond axis to avoid high-energy areas. Finally, we should point out that the bridging proton reduces the *trans*–*gauche* energy difference of n -butane from 5 to

FIG. 7. 3D surface plot of the 2D torsional potential energy surface $E(\Phi_{\text{CCCC}}, \Phi_{\text{HCCX}})$, using CCSD(T)/6-31G(*d,p*) data.

0–2 kJ mol⁻¹ and that the entire 2D surface may fit in an energy range of only 4–8 kJ mol⁻¹.

IV. CONCLUSIONS

The three-center–two-electron CHC bond geometry is a nontrivial challenge for computational chemistry. Our best computed value for the $\theta(\text{C}_3\text{H}_1\text{C}_2)$ bond angle in centrally protonated $\text{C}_4\text{H}_{11}^+$, using the CCSD(T)/cc-pVTZ level of theory, is 122.4°. Lower-level molecular-orbital-based methods result in smaller angles, while lower-level basis sets result in larger angles, so that compromise levels of theory exist: namely, MP2/6-311G(d) and MP2/cc-pVDZ. The density functional methods B3LYP and PW91 produce angles over 30° too large. Our best results for $R(\text{C}_2\text{C}_3)$ and $R(\text{C}_2\text{H}_1)$ are 2.18 and 1.242 Å, respectively.

Four geometrically unique minima exist for centrally protonated $\text{C}_4\text{H}_{11}^+$, but they lie within a 4 kJ mol⁻¹ energy range and sit on a torsional PES which likely fits entirely within a 10 kJ mol⁻¹ energy range. Hence the molecular ion should interconvert rapidly among them in the gas phase at room temperature. The lowest-energy conformer could not be discerned because different levels of theory disagreed on this matter. The two dihedral degrees of freedom Φ_{CCCC} and Φ_{HCCX} are significantly coupled, as can be seen most clearly in our surface plots of fitted potential energy surfaces.

Different levels of theory also give disagreeing results for the small differences in energy between various torsional conformers. A general preference for *gauche* and *trans* structures is seen with MP2 and CCSD(T), although not with B3LYP. The bridging proton generally prefers a staggered position, but the preferred position seems peculiar, since this proton prefers the staggered position between two C–H bonds in the *trans* conformer, but not in the *gauche* conformer. Core-valence correlation effects upon torsional geometries and energies were investigated and found to be insignificant.

ACKNOWLEDGMENTS

The Institute of Computational Discovery (University of Regina) is thanked for computer time on the SGI Onyx 2 supercomputer. NSERC (Canada) is thanked for research funds.

¹V. L. Tal'roze and A. L. Lyubimova, Dokl. Akad. Nauk SSSR **86**, 909 (1952); Chem. Abstr. **47**, 2590 (1953).

²G. G. Meisels, W. H. Hamill, and R. R. Williams, Jr., J. Chem. Phys. **25**, 790 (1956).

³G. G. Meisels, W. H. Hamill, and R. R. Williams, Jr., J. Phys. Chem. **61**, 1456 (1957).

⁴S. Wexler and N. Jesse, J. Am. Chem. Soc. **84**, 3425 (1962).

⁵F. H. Field, J. L. Franklin, and M. S. B. Munson, J. Am. Chem. Soc. **85**, 3575 (1963).

⁶M. S. B. Munson, J. L. Franklin, and F. H. Field, J. Phys. Chem. **68**, 3098 (1964).

⁷F. P. Abramson and J. H. Futrell, J. Chem. Phys. **45**, 1925 (1966).

⁸A. Ding, A. Henglein, and K. Z. Lacmann, Z. Naturforsch. A **23**, 780 (1968).

⁹Z. Herman, P. Hierl, A. Lee, and R. Wolfgang, J. Chem. Phys. **51**, 454 (1969).

¹⁰W. T. Huntress, Jr., J. Chem. Phys. **56**, 5111 (1972).

¹¹J. Weiner, G. P. K. Smith, M. Saunders, and R. J. Cross, Jr., J. Am. Chem. Soc. **95**, 4115 (1973).

¹²K. Hiraoka and P. Kebarle, J. Am. Chem. Soc. **97**, 4179 (1975).

¹³K. Hiraoka and P. Kebarle, J. Chem. Phys. **63**, 394 (1975).

¹⁴M. French and P. Kebarle, Can. J. Chem. **53**, 2268 (1975).

¹⁵K. Hiraoka and P. Kebarle, J. Am. Chem. Soc. **98**, 6119 (1976).

¹⁶K. Hiraoka and P. Kebarle, Can. J. Chem. **58**, 2262 (1980).

¹⁷L. I. Yeh, J. M. Price, and Y. T. Lee, J. Am. Chem. Soc. **111**, 5597 (1989).

¹⁸E. T. White, J. Tang, and T. Oka, Science **284**, 135 (1999).

¹⁹G. A. Olah and A. Molnár, *Hydrocarbon Chemistry* (Wiley, New York, 1995).

²⁰G. A. Olah, G. K. S. Prakash, and J. Sommer, *Superacids* (Wiley-Interscience, New York, 1985).

²¹G. A. Olah, G. K. S. Prakash, R. E. Williams, L. C. Field, and K. Wade, *Hypercarbon Chemistry* (Wiley-Interscience, New York, 1987).

²²G. A. Olah, O. Farooq, and G. K. S. Prakash, *Activation and Functionalization of Alkanes* (Wiley, New York, 1989).

²³W. O. Haag and R. M. Dessau, in Proceedings of the 8th International Congress on Catalysis, Berlin, 1985, Vol. 2, p. 305.

²⁴S. Kotrel, H. Knözinger, and B. C. Gates, Micro. Meso. Mater. **35–36**, 11 (2000).

²⁵J. W. d. M. Carneiro, P. v. R. Schleyer, M. Saunders, R. Remington, H. F. Schaefer, III, A. Rauk, and R. S. Sorensen, J. Am. Chem. Soc. **116**, 3483 (1994).

²⁶S. J. Collins and P. J. O'Malley, J. Chem. Soc., Faraday Trans. **92**, 4347 (1996).

²⁷S. J. Collins and P. J. O'Malley, Chem. Phys. Lett. **228**, 246 (1994).

²⁸J. Hrušák, J. Zabka, Z. Dolejšek, and Z. Herman, Int. J. Mass Spectrom. Ion Processes **167**, 675 (1997).

²⁹R. P. Kirchen, K. Ranganayakulu, A. Rauk, B. P. Singh, and T. S. Sorensen, J. Am. Chem. Soc. **103**, 588 (1981).

³⁰J. Planelles, J. Sánchez-Marín and F. Tomás, J. Mol. Struct.: THEOCHEM **108**, 65 (1984).

³¹M. V. Frash, V. N. Solkan, and V. B. Kazansky, J. Chem. Soc., Faraday Trans. **93**, 515 (1997).

³²M. Boronat, P. Viruela, and A. Corma, J. Phys. Chem. B **101**, 10069 (1997).

³³C. J. A. Mota, P. M. Esteves, A. Ramírez-Solís, and R. Hernández-Lamonedá, J. Am. Chem. Soc. **119**, 5193 (1997).

³⁴P. M. Esteves, C. J. A. Mota, A. Ramírez-Solís, and R. Hernández-Lamonedá, J. Am. Chem. Soc. **120**, 3213 (1998).

³⁵P. M. Esteves, G. G. P. Alberto, A. Ramírez-Solís, and C. J. A. Mota, J. Phys. Chem. A **104**, 6233 (2000).

³⁶P. M. Esteves, G. G. P. Alberto, A. Ramírez-Solís, and C. J. A. Mota, J. Phys. Chem. A **105**, 4308 (2001).

³⁷K. C. Hunter and A. L. L. East, J. Phys. Chem. A **106**, 1346 (2002).

³⁸C. Seitz and A. L. L. East, J. Phys. Chem. A **106**, 11653 (2002).

³⁹M. J. Frisch, G. W. Trucks, H. B. Schlegel *et al.*, GAUSSIAN 98, Revision A.9, Gaussian, Inc., Pittsburgh, 1998.

⁴⁰MOLPRO 2002.3 is a package of *ab initio* programs designed by H.-J. Werner and P. J. Knowles. The authors are R. D. Amos, A. Bernhardsson, A. Berning *et al.*,

⁴¹A. D. Becke, J. Chem. Phys. **98**, 5648 (1993).

⁴²C. Lee, W. Yang, and R. G. Parr, Phys. Rev. B **37**, 785 (1988).

⁴³J. P. Perdew, in *Electronic Structure of Solids '91*, edited by P. Ziesche and H. Eschrig (Akademie Verlag, Berlin, 1991), p. 91.

⁴⁴C. Møller and M. S. Plesset, Phys. Rev. **46**, 618 (1934).

⁴⁵J. A. Pople, R. Seeger, and R. Krishnan, Int. J. Quantum Chem., Quantum Chem. Symp. **11**, 149 (1977).

⁴⁶R. Krishnan, H. B. Schlegel, and J. A. Pople, J. Chem. Phys. **72**, 4654 (1980).

⁴⁷J. Cizek, Adv. Chem. Phys. **14**, 35 (1969).

⁴⁸R. J. Bartlett, J. Phys. Chem. **93**, 1697 (1989).

⁴⁹C. Hampel, K. Peterson, and H.-J. Werner, Chem. Phys. Lett. **190**, 1 (1992).

⁵⁰M. J. O. Deegan and P. J. Knowles, Chem. Phys. Lett. **227**, 321 (1994).

⁵¹M. J. Frisch, J. A. Pople, and J. S. Binkley, J. Chem. Phys. **80**, 3265 (1984).

⁵²T. H. Dunning, Jr., J. Chem. Phys. **90**, 1007 (1989).

⁵³D. E. Woon and T. H. Dunning, Jr., J. Chem. Phys. **103**, 4572 (1995).